ELSEVIER

Journal of Organometallic Chemistry 507 (1996) 31–39

Journal of Organometallic Chemistry

Synthesis, structure and bonding in $Nb_2(\eta^6\text{-mesitylene})_2(\mu\text{-I})_4$ and a new intermediate-valent dinuclear niobium complex, $[Nb_2(\eta^6\text{-mesitylene})_2(\mu\text{-I})_4]I$

Myungok Yoon, Jianhua Lin, Victor G. Young, Jr., Gordon J. Miller *

Ames Laboratory, U.S. Department of Energy, and Department of Chemistry, Iowa State University, Ames, IA 50011-3020, USA

Received 20 December 1994; in revised form 20 April 1995

Abstract

$Nb_2(\eta^6\text{-mesitylene})_2(\mu\text{-I})_4$ (mesitylene ≡ 1,3,5-$C_6H_3(CH_3)_3$ ≡ mes) (**2**) has been synthesized from the reaction of $Nb(\eta^6\text{-mes})_2$ (**1**) with iodine in THF and characterized by NMR, IR, UV-vis spectroscopy, and single crystal X-ray diffraction. The mesitylene ligands in **2** show nonplanar boat conformations, indicating localization of π-electron density in a 1,4-diene fashion, which is supported by a molecular orbital calculation. NMR spectra, however, indicate that **2** undergoes rapid interconversion of boat conformations as well as ring rotation in solution even at −62°C. A cyclic voltammogram of complex **2** exhibits two redox waves. A new intermediate-valent dinuclear complex $[Nb_2(\eta^6\text{-mes})_2(\mu\text{-I})_4]I$ (**3**) was prepared from oxidation of **2** with iodine. The powder EPR spectrum of **3** is discussed, while magnetic studies of **3** exhibit Curie–Weiss paramagnetic behavior at temperatures above 100 K with $\mu_{eff} = 1.77$ BM. Crystal data: **2**, $C_{18}H_{24}I_4Nb_2$, monoclinic, $P21/n$ (No. 14), $a = 10.186(2)$ Å, $b = 8.837(2)$ Å, $c = 12.797(3)$ Å, $\beta = 96.95(2)°$, $V = 1143.3$ Å^3, $Z = 2$, and $d_{calcd} = 2.71$ g cm^{-3}; **3**, $C_{18}H_{24}I_5Nb_2$, monoclinic, $C2/c$, $a = 8.348(2)$ Å, $b = 15.038(3)$ Å, $c = 20.373(4)$ Å, $\beta = 97.25(3)°$, $V = 2537.1(9)$ Å^3, $Z = 4$, and $d_{calcd} = 2.78$ g cm^{-3}.

Keywords: Dinuclear; Niobium; Mesitylene; Arene complexes; Intermediate-valent

1. Introduction

The chemistry of metal sandwich complexes, $M(\eta^6\text{-}C_6H_nR_6 - n)2$ (M = transition metal, $n = 1$–6) has been the focus of many research groups, especially since the synthesis of bis(η^6-benzene)chromium using metal vapors by Timms in 1969. However, the chemistry of group 5 complexes is considerably less developed than that of the 18-electron group 6 complexes [1]. Bis(η^6-arene)niobium complexes have been synthesized mainly by metal vapor techniques [2]. Even though the metal vapor technique provides access to a variety of bis(arene)transition metal complexes not accessible by the conventional Fischer–Hafner synthesis [3a], specialized equipment, available in few laboratories, is required. Thus, a recently reported modification to Fischer–Hafner syntheses [3b–f], which enabled conventional preparations of bis(η^6-mesitylene)niobium (**1**), prompted us to examine the chemistry of **1**. One of our current research interests is to prepare new transition metal solids, such as halides, chalcogenides and chalcogenide halides via low temperature routes by employing organometallic complexes like **1** as a precursor. Complex **1** is anticipated to be very reactive and a good precursor to other higher-nuclearity organometallic complexes owing to an electron-rich niobium atom. In addition, the weakly π-coordinated neutral mesitylene ligands in **1** are expected to be easily removed upon thermolysis. Therefore, investigations of the reactions of **1** with various halogen and chalcogen sources have been attempted. Here, we report the reaction of **1** with iodine as the simplest reagent affording the quadruply bridged dinuclear niobium complex, $Nb_2(\eta^6\text{-mes})_2(\mu\text{-I})_4$(**2**), and a novel iodide salt $[Nb_2(\eta^6\text{-mes})_2(\mu\text{-I})_4]I$ (**3**). Reactions of **1** with chalcogen sources to afford binary solid state compounds at low temperature will be described elsewhere.

* Corresponding author.

SSDI 0022-328X(95)05696-3

Numerous molybdenum complexes, $[Mo_2(\eta^5\text{-}C_5H_nR_{5-n})_2(\mu\text{-}X)_4]$ and $[Mo_2(\eta^6\text{-}C_6H_nR_{6-n})_2(\mu\text{-}X)_4]^{2+}$ (X = halogen, S, SR), which are isoelectronic to **2**, have been synthesized and the electronic structures of a few complexes have been extensively investigated [4]. Only a few organometallic Nb(II) dimers with bridging ligands are known [3a,d,e,h], and their electronic structures have not been investigated. Therefore, in addition to the synthesis, structure, and properties of the dimeric Nb(II) complexes **2** and **3**, we shall briefly address their electronic structures.

2. Results and discussion

2.1. Reactivity of bis(η^6-mesitylene)niobium (1)

The low first ionization potential (5.18 eV) of bis(η^6-mes)niobium (**1**) [2b] and a large negative halfwave potential (−0.495 V vs. SCE) for the $\mathbf{1}/\mathbf{1}^+$ couple [3g] clearly indicate that **1** is a high-energy, electron-rich, and, therefore, very reactive 17-electron complex, like many other zero valent transition metal sandwich complexes. Complex **1** should be handled very carefully in the absence of any oxygen and/or water owing to this reactivity.

The reaction of **1** with elemental iodine afforded a dinuclear d^3–d^3 niobium complex, $Nb_2(\eta^6\text{-mes})_2(\mu\text{-I})_4$ (**2**) with four bridging iodide ions and a total of 34 valence electrons; each Nb atom in **2** has 17 valence electrons, and is anticipated to attain 18 valence electrons by forming a Nb–Nb single bond. A similar molybdenum arene sandwich complex with 18 valence electrons is reported to react with iodine to produce [Mo(mes)$_2$]I through a one-electron redox process [5]. In contrast, $[Nb(mes)_2]^+$ or $[Nb(C_6H_5Me)_2]^+$ cations, in which Nb atoms have only 16 valence electrons, could only be isolated by adding a two-electron ligand such as PMe_3, CO or THF [3e,6a]. However, the Nb(1,3,5-^{t}Bu$_3$C$_6$H$_3$)$_2^+$ cation was found to be stable owing to bulky electron-releasing substituents which sterically protect Nb from further coordination [6b]. According to our electrochemical studies of **1**, iodine can oxidize **1** to $\mathbf{1}^+$. However, any evidence for the formation of Nb(I) compounds could not be obtained; both Nb(mes)$_2$I and $[Nb(mes)_2(THF)]^+$ have been reported by Calderazzo et al. [3e]. To clarify whether the formation of **2** is due to a reaction of either of these complexes with iodine, compound **1** and iodine were reacted in a molar ratio of 2:1 instead of 1:1. However, this reaction exclusively produced **2** as an isolable product, which indicates that complex **1** behaved not as a one-electron, but as a two-electron reductant during the formation of **2**. The exact driving force and the mechanism for the exclusive formation of complex **2** remain unknown at this point.

2.2. Structural study of 2 and 3

Fig. 1 presents a view of a single molecule of complex **2**. The molecular structure is centrosymmetric with the inversion center located at the midpoint between the two niobium atoms. The two niobium atoms are bridged by four iodine atoms forming a compressed octahedral core unit, and the molecule itself can be viewed as two four-legged piano stools [4] sharing a common square base identified by the four bridging iodo ligands. The Nb–Nb bond distance is 2.8546(7) Å and Nb–I distances range between 2.8721(4) and 2.9001(4) Å. Nb–Nb bond distances of 2.632(1)–3.361(1) Å are also reported in a few organometallic dimeric niobium(II) complexes [3e]. A similar complex, $Nb_2(\eta^6\text{-HMB})_2Br_4$ (HMB hexamethylbenzene), was prepared from the reaction of Nb(η^6-HMB)(AlBr$_4$) with THF, and structurally characterized [3e]. The smaller Nb–Nb bond distance of 2.761(2) Å in this complex is reasonable considering the smaller size of the bridging bromide ions compared to iodide ions. A similar compressed octahedral core unit involving bridging Se atoms occurs in a solid state compound, $Nb_2Se_2Cl_6$, but with Nb atoms in the formal oxidation state of + 4. In this case, the reported Nb–Nb bond distance is 2.793 Å [6c]. Therefore, the Nb–Nb bond distance seems to be more

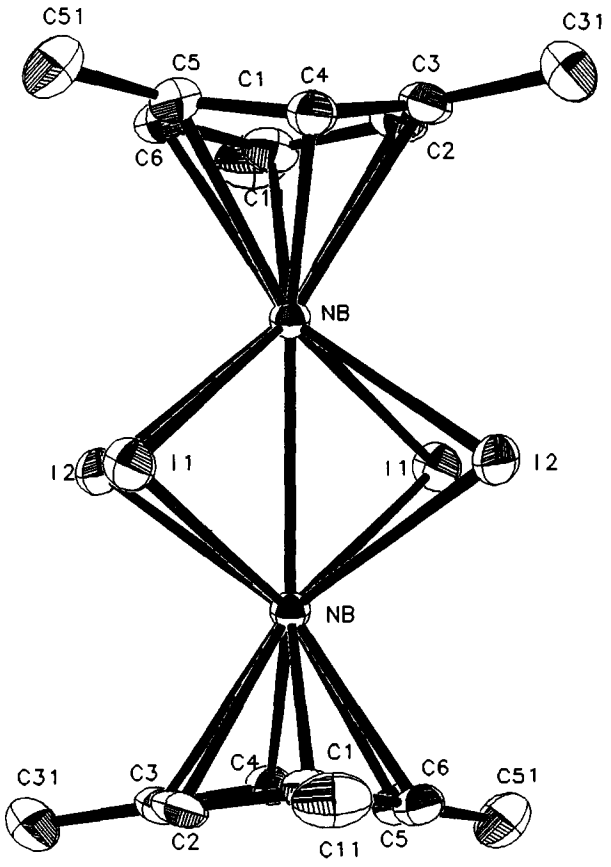

Fig. 1. ORTEP drawing of **2** showing the atom-labeling scheme.

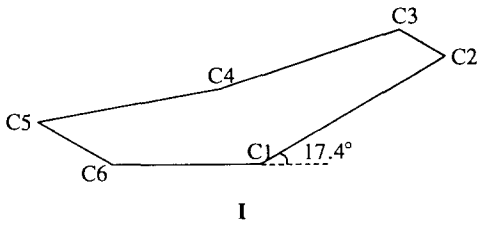

I

Scheme 1.

dependent on the identity of the bridging ligands than on the oxidation state of Nb, which can also be observed in the structural similarities of **2** and $\mathbf{2}^+$ (see Discusion). Even though the observed Nb–Nb bond distance in **2** is short for a Nb–Nb contact, molecular orbital calculations suggest that this Nb–Nb bond has a bond order of one (see Discusion).

The mesitylene ligands are coordinated to the niobium atoms in an η^6-fashion. However, in contrast with the ligands in complex **1** [3f], they have staggered conformations, and are substantially bent away from planarity, which is emphasized in Scheme 1. Deformations of η^6-arene rings are frequently observed in transition metal complexes [7]. The observed dihedral angle between the C1–C2–C3–C4 plane and C1–C6–C5–C4 plane in **2** is 17.4(2)°. The corresponding dihedral angles in $Nb_2(\eta^6\text{-HMB})_2Br_4$, and $[(C_6Me_6)_3Nb_3Cl_6]^{2+}$ are reported to be 19.9(2)° and 17.8°, respectively. This results in a 'boat' conformation for the mesitylene ligand that is further characterized by two carbon atoms (C1 and C4) closer to niobium (Nb–C1 = 2.269(4) Å and Nb–C4 = 2.272(4) Å) than the other four (average distance of Nb–C = 2.413 Å). Carbon–carbon bond distances in the ring manifest another effect of π-coordination of mesitylene to the Nb atoms; shorter C2–C3 and C5–C6 bond distances indicate a 1,4-diene type of localization of π-electron density in the coordinated mesitylene ligand. From the average bond distance of 1.369(6) Å of C2–C3 and C5–C6 bonds, these two C–C bonds can be described as 'double' bonds, and from the average bond distance of 1.443(6) Å of the other four C–C bonds, they can be described as 'single' bonds. The difference (Δ) between $(C\text{–}C)_{avg}$ and $(C\equiv C)_{avg}$, which can be an indicator of the degree of π-localization, is found to be 0.074 Å in **2**. A similar degree of π-localization (Δ = 0.075 Å) was reported in $(C_6Me_6)Ta(DIPP)_2Cl$ (DIPP ≡ 2,6-diisopropylphenoxide) with a greater distortion (dihedral angle = 34.4°) of the ring [7d].

For better understanding of the Nb–Nb bonding and the arene deformation in **2**, extended Hückel calculations were carried out on two models [8]. An idealized molecule was first constructed on the assumption that the arene ring is planar with equal C–C bond distances of 1.428 Å. The observed average values of 2.855 and 2.888 Å were assigned to the Nb–Nb and Nb–I bond distances, respectively. The deformation of the arene ring was then carried out without changing the rest of the structure to maintain C_{2h} point symmetry. Table 1 shows overlap populations calculated for various bonds in the two different molecular structures. In both models, the overlap populations are different not only among the arene C–C bonds (1.01 for C2–C3 and 0.98 for C1–C2), but also among the Nb–C bonds (0.179 for Nb–C1 and 0.141 for Nb–C2). These results suggest that the idealized structure would distort so as to strengthen the bonding interactions within the C2–C3 and Nb–C1 bonds, which is observed in the real structure. The calculated overlap populations of the deformed molecule supports this suggestion.

Table 1
Selected overlap populations in the ideal and deformed structures of **2**

Bond type	Idealized	Deformed
Nb–Nb	0.307	0.307
Nb–I	0.443	0.444
Nb–C1	0.179	0.241
Nb–C2	0.141	0.117
C1–C2	0.982	0.912
C2–C3	1.011	1.089
C1–C11	0.761	0.767

Fig. 2 shows a MO correlation diagram in the vicinity of the HOMO for each model. The calculated HOMO–LUMO energy gap ($a_g \rightarrow a_u$) increases from 1.46 eV to 1.98 eV, which is near the observed transition of 2.2 eV, and is in qualitative agreement with the result of Green et al. on $Cp_2Mo_2Cl_4$ [4e]. As the

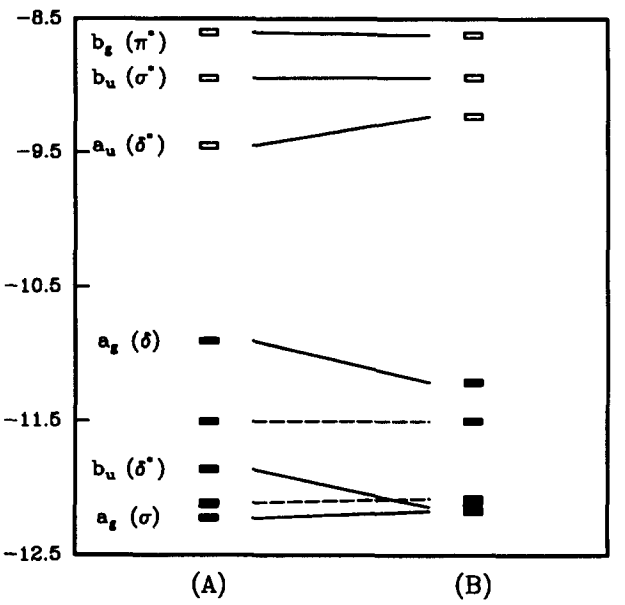

Fig. 2. Molecular orbital energy correlation diagram in the vicinity of the HOMO for (a) an idealized structure of **2** and (b) the observed structure. Occupied levels are darkened.

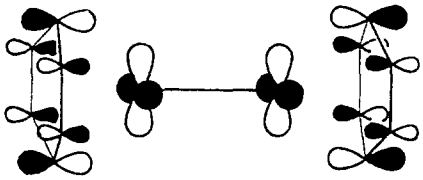

Scheme 2.

distortion of the arene proceeds, the energy levels containing large Nb and C components shift significantly, while the others remain nearly unchanged. Scheme 2 illustrates the niobium and carbon orbital contributions to the HOMO. The iodide component, which is Nb–I π-antibonding, is omitted for clarity. The fragment orbital of the arene is one of its π orbitals that contains four nodes located between C1–C2, C1–C6, C4–C3, and C4–C5. The greatest Nb–C orbital overlap occurs between the p_z orbitals of C1 and C4 with the $4d_{xy}$ orbital of Nb. Clearly, the observed deformation will increase the overlap between the filled metal δ functions and the arene LUMO [15]. As the MO diagram in Fig. 2(b) shows, there are three levels with significant Nb components in the occupied manifold. These levels have Nb–Nb $\sigma(a_g)$, $\delta^*(b_u)$ and $\delta(a_g)$ character. The δ^* orbital (b_u) is occupied due to through-bond coupling effects, which eliminates any iodide component from this orbital. The bond order, based upon this orbital occupation pattern, is close to a single bond, and we can assign the metal as having a d^3 configuration.

The cation in **3**, $[Nb_2(\eta^6\text{-mesitylene})_2(\mu\text{-I})_4]^+$ is almost isostructural to the neutral molecule **2**. The C1 and C2 atoms are also closer to Nb than the other four carbon atoms of the ring, but the differences in distances between these two groups of carbon atoms are reduced (ca. 0.1 Å), giving a lower dihedral angle of 8.7°. Similar phenomena were observed in the case of $(\eta^6\text{-}C_6H_5CH_3)Co(C_6F_5)_2$ and $(\eta^6\text{-}C_6H_5CH_3)Ni(C_6F_5)_2$; the latter, as an 18-electron complex, shows deformation in the arene ring, but the former, as a 17-electron complex, does not [7a]. The average Nb–C ring distance in **3** is larger by 0.03 Å, and all Nb–I bond distances are slightly smaller (0.037 Å) than in **2**, which is possibly due to a greater electrostatic interaction between iodide ions and Nb atoms. The mesitylene ring still exhibits the same π-electron localization with short C2–C3 and C5–C6 bond distances. The Nb–Nb bond distance decreases a little (0.027 Å) upon oxidation from **2** to **3**.

2.3. NMR study of 2

Complex **2** is insoluble in petroleum ether, sparingly soluble in dichloromethane and benzene, soluble in THF, and most soluble in chloroform, which, therefore, has been used as an NMR solvent. Ring protons in **2** experience a characteristically large upfield shift (4.54 ppm) from the uncomplexed mesitylene resonance (6.80 ppm) owing to quenching of the ring current, metal–ligand bond anisotropy, and changes in hybridization of the ring carbon atoms. Methyl protons experience smaller changes in chemical shift (0.29 ppm) than ring protons owing to the greater separation from Nb. Identical trends were observed in $^{13}C\{^1H\}$ NMR spectra.

The calculated total energy difference of 13.4 kJ mol^{-1} between planar and distorted arene (Fig. 2) is small enough to be readily surmounted at room temperature on the NMR timescale. In fact, the solution NMR spectrum ($CDCl_3$) showed only one resonance for each type of site (methyl or mesityl) for complex **2**, indicating that the puckered rings are fluxional in solution at room temperature and also that the mesitylene ligand is rotating rapidly around the molecular axis. Cooling the solution to −62°C did not affect the spectrum except for a small change in the chemical shift due to the temperature change, which indicates that the barriers for both ring flip-flopping and ring rotation are small enough to be overcome even at low temperature.

Solid-state $^{13}C\{^1H\}$ NMR spectra (75 MHz) of **2** with cross polarization magic angle spinning at 2.5 and 3.25 kHz show two different resonances for methyl carbons at 23.89 and 28.59 ppm in the ratio of 1:2. This observation strongly supports the hypothesis that there are two different types of methyl carbons in the solid state, even though they seem to be in the same chemical environment in solution due to rapid rotation and ring flip-floppings. The other carbon resonances are not as well resolved as those for the methyl carbon atoms, but they also strongly support the deformed structure of the complexed mesitylene ligands in **2**.

2.4. Electrochemical properties of complex 2

Fig. 3 shows a cyclic voltammogram of **2** in THF. Complex **2** exhibits two successive quasi-reversible one-electron redox waves, one at $E_{1/2} = 0.213$ V vs. SCE for the $[2]/[2]^+$ couple and one at $E_{1/2} = 0.593$ V vs SCE for the $[2]^+/[2]^{2+}$ couple. $[2]^+$ can represent either a mixed-valent complex ion, $[(\eta^6\text{-mes})Nb^{2+}(\mu\text{-I})_4Nb^{3+}(\eta^6\text{-mes})]^+$, or an intermediate-valent complex ion, $[(\eta^6\text{-mes})Nb^{2.5+}(\mu\text{-I})_4Nb^{2.5+}(\eta^6\text{-mes})]^+$; a cyclic voltammogram alone can not differentiate the latter from the former. Two redox waves are well-separated ($\Delta E_{1/2} = 0.380$ V), even though they are much closer to each other compared with those of $Cp_2^*Mo_2Br_4$, which is isoelectronic to **2** and has two redox waves 1.03 V apart [3c]. According to our electrochemical investigations, iodine, whose reduction potential to iodide ion is 0.2943 V vs. SCE, can oxidize **2** to $[2]^+$. In fact, **3**, which can be expressed as an iodide salt of the $[2]^+$, has been prepared from the reaction of **2** with

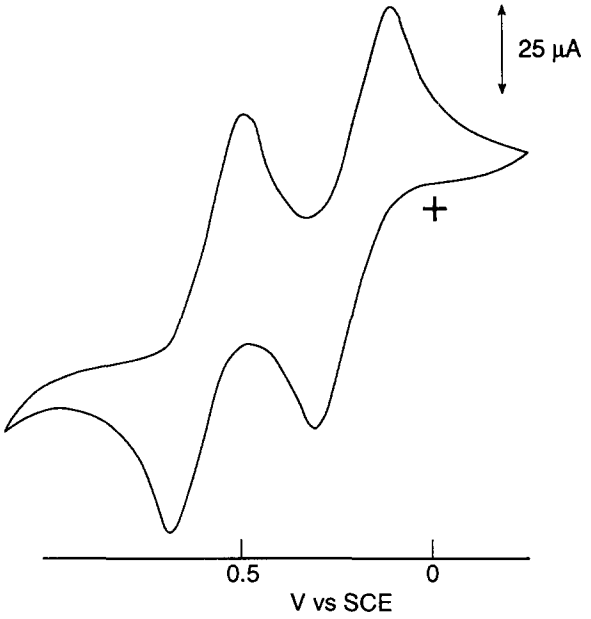

Fig. 3. Cyclic voltammograms of **2** (1 mM) in THF, referenced to SCE (0.1 M $[NBu^n_4][PF_6]$, scan rate 0.05 V s^{-1}).

iodine. However, iodine does not have enough oxidizing power to oxidize $[2]^+$ to the dication $[2]^{2+}$.

2.5. Magnetic results of $[Nb_2(\eta^6\text{-}mes)_2(\mu\text{-}I)_4]I$ (3)

The magnetic susceptibility for complex **3** has been measured over the temperature range 6–296 K. The susceptibility essentially obeys the Curie–Weiss relation and the Weiss constant is nearly zero ($\theta = 2$ K) as expected from very weak magnetic interactions between paramagnetic cations in the solid. The effective magnetic moment above 100 K was calculated to be 1.77 BM from the Curie constant (0.393 emu K mol^{-1}), which is very close to the predicted spin-only magnetic moment (1.73 BM).

2.6. EPR spectrum of 3

The powder EPR spectrum of **3** (Fig. 4) was broad, and unsymmetrical with two different anisotropic g factors ($g_\perp = 2.076$ and $g_\parallel = 2.234$), typical of powder samples with axial symmetry at room temperature [9a,b]; similar g factors ($g_\perp = 2.14$ and $g_\parallel = 2.35$) were reported for a similar dinuclear cation, $[Cp^*_2Mo_2(\mu\text{-}I)_4]^+$ [4g]. No hyperfine coupling to the Nb nucleus ($I = 9/2$) was observed. Many attempts to obtain an expected 19-line EPR solution spectrum were not successful owing to the lack of solubility and/or stability of complex **3** in any solvent. The powder EPR spectrum of bis(η^6-mes)niobium (**1**), which gave a well-resolved 10-line EPR spectrum in hexanes, showed a very similar line shape to that of **3** with two different anisotropic g factors ($g_\perp = 1.980$ and $g_\parallel = 2.003$) without any hyperfine structure [3g].

Charge delocalization in dinuclear metal complexes depends on the extent of bridging between two metal atoms [7d,e]. In an isoelectronic complex ion, $[Cp^*_2Mo_2(\mu\text{-}Br)_4]^+$, the authors assigned two different oxidation states to Mo although the ion was reported to have a Mo–Mo single bond (2.643 Å) [4b]. It seems to be a general assumption that the unpaired electron in **3** should be delocalized between two chemically equivalent Nb atoms which are connected through a single bond, giving an intermediate-valent complex ion. However, the chemical equivalence of the two Nb atoms in **3** is exclusively based on the time-averaged X-ray single crystal structure. Therefore, we hoped to investigate in detail the chemical equivalence of the two Nb atoms

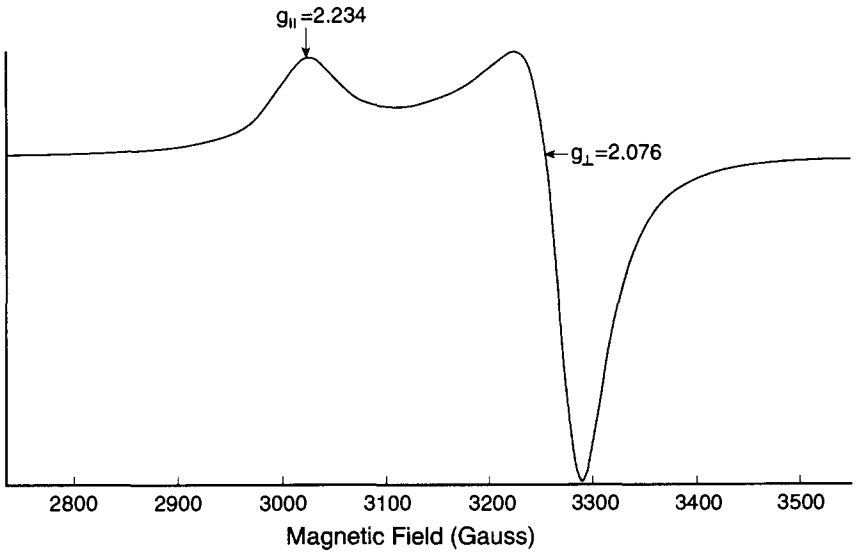

Fig. 4. Powder EPR spectrum of **3** at 9.47 GHz at room temperature.

relative to the unpaired electron via an EPR spectroscopy [9c].

In order to obtain a well-resolved solution EPR spectrum, controlled potential electrolysis of **2** was performed in THF with 0.1 M $[NBu^n_4][PF_6]$ as a supporting electrolyte at 0.4 V in order to oxidize **2** to $\mathbf{2}^+$ electrochemically and to produce $[\mathbf{2}^+][PF_6]$, which is expected to be more soluble than $_3$. As electrolysis proceeded, the pale brown solution changed color to pale red along with formation of a red precipitate. The resulting pale red solution with λ_{max} at 534 nm was unfortunately EPR-silent at 25 and −193°C. However, a powder EPR spectrum of the red precipitate, which was characterized as $[\mathbf{2}^+][PF_6]$ by IR spectroscopy and elemental analyses, shows a pattern similar to that of **3**, and its magnetic susceptibility obeys the Curie–Weiss law with μ_{eff} of 1.89 BM. These observations strongly indicate that $\mathbf{2}^+$ is paramagnetic, but EPR-silent owing to either instability in solution or fast relaxation.

Further efforts to elucidate the delocalization of the unpaired electron density in **3** employing IR spectroscopy was not possible owing to the absence of any characteristic strong absorption frequency which involves niobium atoms.

3. Experimental section

All manipulations were carried out under an atmosphere of dry deoxygenated argon either in a dry box (Vacuum Atmospheres Co.) or by employing standard Schlenk techniques [10]. Tetrahydrofuran (THF) was distilled from and stored over Na–K alloy, and vacuum-distilled immediately prior to use. $CDCl_3$ was distilled from P_2O_5. $NbCl_5$ (Johnson Matthey Co., Inc.) was sublimed under vacuum at 100°C. $Nb(\eta^6\text{-mes})_2$ (**1**) was prepared according to the literature method [3d,e].

^{1}H NMR spectra were recorded on a Nicolet NT-300 or Varian VXR-300 spectrometer using the proton impurity of the solvents as an internal reference. Mass spectra were obtained on a Finnigan 4000 instrument. FT–IR spectra were recorded on an IBM/Bruker IR-98 or a Digilab FTS-7 FTIR spectrometer as CsI pellets. Visible spectra were recorded on Hewlett Packard 8452A Diode Array spectrometer. EPR measurements were performed with a Bruker ER200 spectrometer at X-band frequency. Elemental analyses were performed by Galbraith Laboratories, Inc., Knoxville, TN.

Cyclic voltammograms of **1** and **2** were recorded in THF solutions (1 mM) with 0.1 M $[NBu^n_4][PF_6]$ as supporting electrolyte by employing a CV-27 potentiostat (Bioanalytical Systems, Inc., West Lafayette, IN). A platinum electrode was employed as the working electrode and a platinum wire as the counter electrode. Potentials are referenced against the standard calomel electrode.

The magnetic response of complex **3** was measured over the range 6–296 K using a Quantum Design DC SQUID magnetometer at constant field strength (3 Tesla). Complex **3** (15 mg) was ground to a fine powder to minimize possible anisotropic effects, and loaded in a fused silica tube. Corrections for the diamagnetism of the sample holder and core diamagnetism were applied from Pascal's constants [11].

3.1. Preparation of $Nb_2(\eta^6\text{-mes})_2(\mu\text{-}I)_4$ (2)

A solution of iodine (376 mg, 1.48 mmole) in THF (10 ml) was added dropwise over 15 min to a previously filtered THF (30 ml) solution of **1** (593 mg, 1.78 mmole). The reaction mixture was stirred for 12 h at room temperature and then cooled to −30°C, affording **2** as red diamagnetic microcrystalline precipitates. Complex **2** was filtered, washed with 2 × 5 ml of cold THF, dried under vacuum and collected in the dry box (69 mg). The volume of the filtrate was decreased to ca. 10 ml under reduced pressure and kept at −30°C for 12 h, affording another crop of complex **2**, as needle-shaped dark red crystals which were collected by the same procedure. Total yield: 311 mg, 45%. Anal. Calc. for $C_{12}H_{24}I_4Nb_2$: C, 23.15; H, 2.57; Nb, 19.89. Found: C, 23.31; H, 2.83; Nb, 19.92. ^{1}H NMR ($CDCl_3$): δ 2.00 (s, 18 H, $-CH_3$), 4.56 (s, 6 H, ring proton), ^{1}H NMR ($CDCl_3$, −62°C): δ 1.98, 4.54 ppm. $^{13}C\{^1H\}$ NMR ($CDCl_3$): 24.40 (s, CH_3), 105.89 (s, C–CH_3), 112.37 (s, C–H) ppm. EIMS (70 eV): m/e 120 (mesitylene$^+$), 127 (I^+). CIMS (NH_3): m/e 935 ($M^+ + H^+$), 953 ($M^+ + NH_4^+$). IR (CsI pellet) 3036 w, 2963 m, 2910 m, 2721 w, 1717 w, 1636 w, 1558 m, 1499 w, 1437 m, 1373 s, 1288 w, 1138 m, 891 w, 874 m, 706 w, 634 m, 564 m, 523 w, 481w, 395 m, 324 w cm^{-1}. UV (THF): $\lambda_{max}(\varepsilon) = 254$ (5418), 310 (7427), 370 (6943), 555 nm (236).

3.2. Preparation of $[Nb_2(\eta^6\text{-mes})_2(\mu\text{-}I)_4]I$ (3)

THF (20 ml) was distilled into a flask containing complex **2** (76 mg, 0.23 mmole) and I_2 (11 mg, 0.043 mmole). After the reaction mixture was stirred for 12 h at room temperature, a dark red-brown solid **3** was filtered, washed with THF (2 × 5 ml) to remove any unreacted starting reagents, dried under vacuum and collected in the dry box. Yield: 64 mg (74%). Anal. Calc. for $C_{12}H_{24}I_5Nb_2$: C, 20.38; H, 2.28. Found: C, 20.18; H, 2.22. IR (CsI pellet): 3053 w, 2984 w, 1541 s, 1443 m, 1375 s, 1157 w, 1032 m, 1011 m, 908 w, 570 w, 502 w, 285 w, 250 m.

3.3. Preparation of $[Nb_2(\eta^6\text{-mes})_2(\mu\text{-}I)_4]PF_6$

Compound **2** (25 mg, 0.027 mmole) and dried $[NBu^n_4][PF_6]$ (387 mg, 1.0 mmole) were dissolved in

Table 2
Crystallographic data for $Nb_2(\eta^6\text{-mes})_2(\mu\text{-I})_4$ (2) and $[Nb_2(\eta^6\text{-mes})_2(\mu\text{-I})_4$ (3)

	2	3
Formula	$C_{18}H_{24}I_4Nb_2$	$C_{18}H_{24}I_5Nb_2$
Fw	933.8	1060.7
Space group	$P2_1/n$	$C2/c$
a (Å)	10.186(2)	8.348(2)
b (Å)	8.837(2)	15.038(3)
c (Å)	12.797(3)	20.373(4)
β (deg)	96.95(2)	97.25(3)
V (Å^3)	1143.3(8)	2537.1(9)
Z	2	4
d_{calcd} (g cm^{-3})	2.71	2.78
λ (Å)	0.71073	0.71073
μ (cm^{-1})	64.4	69.89
T (°C)	−50(1)	27
Transm coeff	0.999–0.728	0.927–0.592
$R(F_0)$ [a]	0.018	0.065
$R_w(F_0)$ [b]	0.025	0.066

[a] $R(F_0) = \Sigma\|\|F_0| - |F_c\|\|/\Sigma|F_0|$. [b] $R_w(F_0) = [\Sigma w(|F_0| - |F_c|)^2/\Sigma w|F_0|^2]^{1/2}$; $w = 1/\sigma^2(|F_0|)$.

THF (10 ml), transferred into an electrochemical cell, and electrolyzed at 0.4 V (vs. SCE) for 2 h by employing a glassy carbon electrode (o.d. = 8.0 mm) as the working electrode and a Pt wire (o.d. = 1.5 mm) as the counter electrode. As electrolysis proceeded, the pale brown solution changed color to pale red along with formation of a red precipitate, which was filtered, washed with THF (2 × 10 ml) to remove $[NBu^4_n][PF_6]$ completely, dried under vacuum, and collected. Yield: 22 mg (76%). Anal. Calc. for $C_{12}H_{24}F_6I_4Nb_2P$: C, 20.04; H, 2.24. Found: C, 19.48; H, 2.36. IR (CsI pellet): 3098 w, 3060 m, 2966 s, 2934 m, 2877 w, 1542w, 1458 w, 1384 w, 1303 w, 1263 w, 1099 w, 1032 m, 837 s, 739 w, 558 s.

3.4. Crystallographic studies of 2 and 3

Crystals of **2** suitable for single crystal X-ray diffraction were mounted into glass capillaries in an Ar-filled glove box. After the quality of the crystals was checked with Weissenberg photographs, data were collected on an Enraf–Nonius CAD4 diffractometer at −50 ± 1°C. Pertinent crystallographic data are listed in Table 2. The space group $P2_1/n$ was selected based on the systematic absences, and the crystal structure was solved by direct methods [12]. The following refinement gave a very good residual value which enabled location of at least one hydrogen atom of every methyl group from the difference Fourier map. These peaks were then used to generate ideal, riding hydrogen positions with C–H distances equal to 0.95 Å, and these were refined with isotropic thermal parameters. The mesitylene hydrogens were also refined as riding, but the thermal parameters were fixed at the adjacent carbon's isotropic equivalent value. The final refinement gave a residual value of 1.8%. Positional parameters of the crystal structure for **2** are listed in Table 3, and selected bond distances and angles are in Table 5 [13].

Table 3
Positional displacement parameters for **2**

Atom				
Nb	1399.3(3)	4799.4(4)	4914.4(3)	6.7(1)
I1	317.5(3)	2196.2(3)	5028.1(2)	25.8(1)
I2	116.6(3)	5019.1(3)	3019.9(2)	25.3(1)
C1	6823(4)	5702(5)	5628(3)	26.6(1)
C2	6524(4)	6069(5)	4530(3)	27.6(1)
C3	6549(4)	5028(4)	3740(3)	25.6(1)
C4	6895(4)	3493(5)	4027(3)	24.2(9)
C5	6819(4)	3017(5)	5098(3)	26.2(10)
C6	6811(4)	4097(5)	5865(3)	28.0(10)
C11	6724(4)	6884(5)	6465(3)	39.5(11)
C31	6226(5)	5426(6)	2605(3)	38.0(13)
C51	6789(5)	1349(5)	5338(4)	39.4(11)

Equivalent isotropic U defined as one third of the trace of the orthogonalized U_{ij} tensor.

Growing single crystals of **3** by recrystallization was unsuccessful owing to the lack of solubility and/or stability of **3** in any solvent. Crystals could form by layering equimolar solutions of iodine in ether onto THF solution of **2**. Surprisingly, single crystals of **3** could also be grown from a saturated THF solution of **2** which was stoppered with a septum and left undisturbed for 7 days. During this period, black needle-shaped crystals formed, which were collected by cannulating out the supernatant solution. The homogeneity of these crystals was confirmed later by comparing the observed X-ray powder diffraction pattern (Enraf–Nonius Guinier camera, Cu Kα_1 radition) with the calculated X-ray powder pattern using the crystallographic parameters of **3**. A crystal of complex **3** was mounted in a glass capillary in an Ar-filled glove box, and data were collected on a Siemens P4 diffractometer at 27 ± 1°C.

Table 4
Positional displacement parameters for **3**

Atom	x	y	z	U_{eq}
I1	1270(2)	8964(1)	166(1)	44(1)
I2	328(2)	6743(1)	514(1)	44(1)
Nb1	3416(2)	7575(1)	630(1)	24(1)
I3	0	5824(2)	2500	52(1)
C1	3262(26)	8004(16)	1740(11)	33(8)
C2	3666(30)	7103(16)	1788(12)	37(8)
C3	4982(28)	6759(15)	1538(12)	39(8)
C4	6016(27)	7362(16)	1223(11)	38(8)
C5	5736(29)	8291(16)	1266(12)	38(8)
C6	4389(32)	8614(16)	1504(11)	43(9)
C11	1776(30)	8341(18)	2029(13)	54(10)
C31	5481(33)	5781(15)	1601(12)	46(9)
C51	7035(36)	8894(17)	1079(14)	67(12)

Equivalent isotropic U defined as one third of the trace of the orthogonalized U_{ij} tensor.

Table 5
Selected bond distances (Å) and angles (deg) for **2** and **3**

Atoms	Distance (**2**)	Distance (**3**)
Nb–Nb	2.8546(7)	2.828(4)
Nb–I1	2.8826(5)	2.847(3)
Nb–I1	2.8721(4)	2.836(3)
Nb–I2	2.8966(5)	2.857(3)
Nb–I2	2.9001(4)	2.865(3)
Nb–C1	2.269(4)	2.370(23)
Nb–C2	2.392(4)	2.446(24)
Nb–C3	2.430(4)	2.454(23)
Nb–C4	2.272(4)	2.368(21)
Nb–C5	2.436(4)	2.441(23)
Nb–C6	2.393(4)	2.431(23)
C1–C2	1.438(6)	1.397(34)
C1–C6	1.451(7)	1.440(35)
C2–C3	1.369(6)	1.369(35)
C3–C4	1.438(6)	1.455(34)
C4–C5	1.445(6)	1.421(34)
C5–C6	1.369(6)	1.369(37)
Atoms	Angle (**2**)	Angle (**3**)
Nb–I1–Nb	59.48(1)	59.6(1)
Nb–I2–Nb	59.01(1)	59.3(1)
I1–Nb–I1	120.52(1)	120.4(1)
I1–Nb–I2	76.31(1)	75.2(1)
I2–Nb–I2	120.99(1)	120.7(1)

Lorentz and polarization corrections were applied to the measured intensities. In addition, during the course of the diffraction experiment, the standard reflections decayed to 92% of their original value, and a linear correction based on this decay was applied to the data. Pertinent crystallographic data for **3** are listed in Table 2 and positional parameters are in Table 4. Selected bond distances and angles are listed in Table 5 and the view of unit cell packing is shown in Fig. 5.

The space group $C2/c$ was chosen based on systematic absences and intensity statistics. This assumption proved to be correct by a successful direct-methods solution and subsequent refinement. All non-hydrogen atoms were placed directly from the E-map and refined with anisotropic thermal parameters. The hydrogens of the coordinated mesitylene were refined as riding-atoms with C–H distances of 0.96 Å with individual isotropic thermal parameters.

Data collection and structure solution were done at the Iowa State Molecular Structure Laboratory. Refinement calculations were performed on a Digital Equipment MicroVAX 3100 computer using the SHELXTL-Plus programs [14].

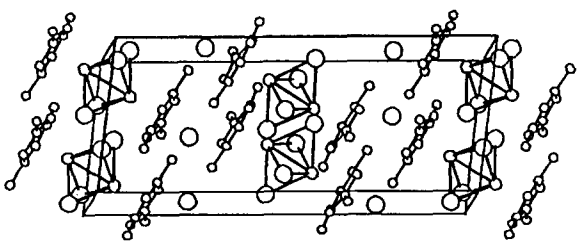

Fig. 5. View of the unit cell packing in complex **3**. The view is down the z axis.

Acknowledgments

This research was supported by the Chemical Sciences Division, Office of Basic Energy Sciences, U.S. Department of Energy, under Contract W-7405-Eng-82. We thank J.E. Ostenson for magnetic measurements and C.J. Zhong for assistance in the electrochemical measurements.

References and notes

[1] (a) W.E. Silverthorn, *Adv. Organomet. Chem., 13* (1975) 47; (b) J.P. Collman, L.S. Hegedus, J.R. Norton and R.G. Finke, *Principles and Applications of Organotransition Metal Chemistry*, University Science Books, Mill Valley, CA, 1987; (c) E.L. Muetterties, J.R. Bleeke, E.J. Wucherer and T.A. Albright, *Chem. Rev., 82* (1982) 499.

[2] (a) F.G.N. Cloke and M.L.H. Green, *J. Chem. Soc., Dalton Trans.* (1981) 1938; (b) F.G.N. Cloke and M.L.H. Green, *J. Organomet. Chem., 200* (1980) 119; (c) F.G.N. Cloke, M.L.H. Green and D.H. Price, *J. Chem Soc., Chem. Commun., 431* (1978); (d) J.A. Bandy, K. Frout, F.G.N. Cloke, H.C. de Lemos and J.M. Wallis, *J. Chem. Soc., Dalton Trans.* (1988) 1475.

[3] (a) E.O. Fischer and F. Röhrscheid, *J. Organomet. Chem., 6* (1966) 53; (b) P. Powell, *Principles of Organometallic Chemistry*, Chapman and Hall, London, 2nd edn., 1988, p. 311; (c) F. Calderazzo, G. Pampaloni, L. Rocchi, J. Strähle and K. Wurst, *Angew. Chem., Int. Ed. Engl., 30* (1991) 102; (d) F. Calderazzo and G. Pampalomi, *J. Organomet. Chem., 423* (1992) 307; (e) F. Calderazzo, G. Pampaloni and L. Rocchi, *J. Organomet. Chem., 413* (1991) 91 and refs. therein; (f) F. Calderazzo, F. Gingl, G. Pampaloni, L. Rocchi and J. Strahle, *Chem. Ber., 125* (1992) 1005; (g) in this work; (h) M.L.H. Green, D. O'Hare, P. Mountford and J.G. Watkin, *J. Chem. Soc., Dalton Trans.* (1991) 1705.

[4] (a) W.E. Silverthorn, *J. Chem. Soc., Chem. Commun.* (1978) 1009; (b) P.D. Grebenik, M.L.H. Green, A. Izquierdo, V.S.B. Mtetwa and C.K. Prout, *J. Chem. Soc., Dalton Trans.* (1987) 9; (c) W. Tremel, R. Hoffmann and E.D. Jemmis, *Inorg. Chem., 28* (1989) 1213; (d) B.E. Bursten and R.H. Cayton, *Inorg. Chem., 28* (1989) 2846; (e) J.C. Green, M.L.H. Green, P. Mountford and M.J. Parkington, *J. Chem. Soc., Dalton Trans.* (1990) 3407; (f) M.L.H. Green, J.D. Hubert and P. Mountford, *J. Chem. Soc., Dalton Trans.* (1990) 3793; (g) R. Poli, J.C. Gordon, J.U. Desai and A.L. Rheingold, *J. Chem. Soc., Chem. Commun.* (1991) 1518; (h) M.L.H. Green and P. Mountford, *Chem. Soc. Rev., 29* (1992); (i) J.U. Desai, J.C. Gordon, H.-B. Kraatz, B.E. Owens-Waltermire, R. Poli and A.L. Rheingold, *Angew. Chem., Int. Ed. Engl., 32* (1993) 1486; (j) K. Fromm and E. Hey-Hawkins, *Z. Anorg. Allg. Chem., 619* (1993) 261; (k) F. Abugideiri, G.A. Brewer, J.U. Desai, J.C. Gordon and R. Poli, *Inorg. Chem., 33* (1994) 3745; (l) J.U. Desai, J.C. Gordon, H.-B. Kraatz, V.T. Lee, B.E. Owens-Waltermire, R. Poli, A.L. Rheingold and C.B. White, *Inorg. Chem., 33* (1994) 3752; (m) J.H. Shin and G. Parkin, *Polyhedron, 13* (1994) 1489.

[5] E.O. Fischer, F. Scherer and H.O. Stahl, *Chem. Ber., 93* (1960) 2065.

[6] (a) J.A. Bandy, K. Prout, F.G.N. Cloke, H.C. de Lemos and J.M. Wallis, *J. Chem. Soc., Dalton Trans.* (1988) 1475; (b) F.G.N. Cloke, K.A.E. Courtney, A.A. Sameh and A.C. Swain, *Polyhedron, 8* (1989) 1641; (c) J. Rijnsdorp, G.J. de Lange and G.A. Wiegens, *J. Solid State Chem., 30* (1979) 365.

[7] (a) L.J. Radonovich, F.J. Koch and F.J. Albright, *Inorg. Chem., 19* (1980) 3373 and refs. therein; (b) D.J. Arney, P.A. Waxler and D.E. Wigley, *Organometallics, 9* (1990) 1282 and refs. therein; (c) P.A. Wexler and D.E. Wigley, *Organometallics, 10* (1991) 2319; (d) D.P. Smith, J.R. Strickler, S.D. Gray, M.A. Bruck, R.S. Holmes and D.E. Wigley, *Organometallics, 11* (1992) 1275; (e) M.A. Bruck, A.S. Copenhaver and D.E. Wigley, *J. Am. Chem. Soc., 109* (1987) 6525. We prefer the term "intermediate-valent" to "mixed-valent" used by authors for the charge-delocalized ion; (f) N.V. Oder, Jr., W.E. Geiger, T.E. Bitterwolf and A.L. Rheingold, *J. Am. Chem. Soc., 109* (1987) 5680.

[8] R. Hoffmann, *J. Chem. Phys., 39* (1963) 1397. The atomic orbital parameters for the calculation are: Nb: $\zeta(5s) = 1.89$, $H_{ii}(5s) = -8.96$ eV, $\zeta(5p) = 1.85$, $H_{ii}(5p) = -4.99$ eV, $\zeta_1(4d) = 4.08$ ($c_1 = 0.6401$), $\zeta_2(4d) = 1.64$ ($c_2 = 0.5516$), $H_{ii}(4d) = -9.83$ eV; I: $\zeta(5s) = 2.66$, $H_{ii}(5s) = -18.00$ eV, $\zeta(5p) = 2.32$, $H_{ii}(5p) = -12.70$ eV; C: $\zeta(2s) = 1.63$, $H_{ii}(2p) = -21.40$ eV, $\zeta(2p) = 1.63$, $H_{ii}(2p) = -11.40$ eV; H: $\zeta(1s) = 1.30$, $H_{ii}(1s) = -13.60$ eV.

[9] (a) L.A. Blumenfeld, V.V. Voevodski and A.G. Semenov, *Electron Spin Resonance in Chemistry*, Wiley and Sons, New York, 1973; (b) F.K. Kneubühl, *J. Chem. Phys., 33* (1960) 1074; (c) while this article was being written, a 19-line solution EPR spectrum of a dinuclear Nb complex cation, $Nb_2S_4(S_2CNEt_2)^{4+}$, was reported [9d] which is indicative of an intermediate-valent ion with two Nb atoms in the same formal oxidation state of +3.5; (d) M. Sokolov, A. Virovets, V. Nadolinnyi, K. Hegetschweiler, V. Fedin, N. Podberezskaya and V. Fedorov, *Inorg. Chem., 33* (1994) 3503.

[10] D.F. Shriver and M.A. Dresdon, *The Manipulation of Air-Sensitive Compounds*, Wiley, New York, 1986.

[11] P.W. Selwood, *Magnetochemistry*, Interscience, New York, 1956.

[12] CAD4-SDP: Enraf-Nonius Structure Determination Package; Enraf-Nonius: Delft, Holland. Neutral-atom scattering factors and anomolous scattering corrections were taken from *International Tables for X-ray Crystallography*, Vol. IV, Kynoch, Birmingham, England, 1974.

[13] Further details of the crystal structures of **2** and **3** are available on request: anisotropic replacement parameters, bond distances and bond angles (12 pages), and tables of observed and calculated structure factors (5 pages for **2** and 4 pages for **3**).

[14] SHELXTL-PLUS, Siemens Analytical Xray, Inc., Madison, WI.

[15] P. Kubácek, R. Hoffmann and Z. Havlas, *Organometallics, 1* (1982) 180.